Delay-Dependent Stability of Load Frequency Control with Adjustable Computation Accuracy and Complexity

Li Jin[a,b,c], Yong He[a,b,c], Chuan-Ke Zhang[a,b,c,*], Lin Jiang[d], Wei Yao[e], Min Wu[a,b,c]

[a]School of Automation, China University of Geosciences, Wuhan 430074, China
[b]Hubei Key Laboratory of Advanced Control and Intelligent Automation for Complex Systems, Wuhan 430074, China
[c]Engineering Research Center of Intelligent Technology for Geo-Exploration, Ministry of Education, Wuhan 430074, China
[d]Department of Electrical Engineering and Electronics, University of Liverpool, Liverpool L69 3GJ, United Kingdom
[e]State Key Laboratory of Advanced Electromagnetic Engineering and Technology, Huazhong University of Science and Technology, Wuhan 430074, China

Abstract

Cyber-physical power systems (DCPPS) utilize wide-area measurement system, where communication networks employed in the control loop introduce time delays inevitably. The existing studies focus on either computation accuracy or efficiency for investigating the delay-dependent stability of large-scale DCPPS. Whereas, the requirements for calculation accuracy and efficiency vary from the demand for online stability analysis and offline controller design. This paper investigates the demand-oriented stability of the DCPPS and takes load frequency control (LFC) systems as typical examples. Novel regulation schemes have been proposed with adjustable conservatism and computation complexity. Different from existing studies, this paper establishes regulated stability criteria by constructing variable Lyapunov-Krasovskii functionals and using compatible integral inequalities for estimations. Then, an algorithm is designed by introducing a threshold parameter to calculate accurate delay margins or to realize high computation efficiency flexibly. Case studies are complemented on the two-area LFC scheme and IEEE 39-bus system. It is illustrated that the proposed method can realize on-demand adjustments for real power systems, i.e., setting the threshold parameter to zero achieves almost accurate delay margins like the frequency-domain method, which guides the offline controller design with desired performance; less computation complexity is achieved with a relatively large threshold parameter, and thus, the proposed method is applicable for online stability analysis.

Keywords: Load frequency control, delay-dependent stability, adjustable accuracy and complexity.

1. Introduction

Most power system control applications utilize local signals, where time delays in the control loops are always neglected and approximated by simple lag blocks. Recently, a growing research interest has been paid on modeling, analysis and control of delayed cyber-physical power systems (DCPPS) due to the advent of phasor measurement unit (PMU)-based wide-area measurement system (WAMS) [1]. By globally observing remote signals, load frequency control (LFC) aims to maintain the frequency and power interchanges with neighborhood areas at scheduled values [2]-[4]. The traditional LFC employs dedicated communication channels to transmit information, where small delays are induced and ignored normally [5, 6]. When a communication fault happens, a fault counter will be triggered to record the fault period. The LFC scheme will be suspended or stopped when the counted steps reach the predefined upper bound [7]. The data drop caused by the communication fault can be converted to an equivalent time-varying delay [8]. Time delays degrade the dynamic performance of the LFC systems and even cause instability with the area control error (ACE) being far away from zero [9]-[11]. That is, the control areas cannot follow the control performance standards of CPS1 and CPS2 adopted by the North American Electric Reliability Council (NERC) [12, 13]. Thus, it is essential to find the maximal admissible upper bounds called delay margins, within which the system remains stable [14].

Frequency-domain methods realize the exact delay upper bounds for the power system with constant delays, but they are limited to the analysis with constant delays [15]. In a modern power system, open communication networks are preferred to support the increasing decentralized property of control services, where constant and time-varying delays are introduced [16, 17]. Time-domain methods based on the Lyapunov stability theory together with linear matrix inequality techniques (LMIs) are alternative approaches [18, 19]. Although time-domain methods have inherited conservatism characteristics, they can be conveniently applied to systems with single or multiple, constant or time-varying delays [20].

To lessen the conservatism, more efforts have been paid

☆This work was supported in part by the National Natural Science Foundation of China under Grants 62203410, 62022074, and 61973284, in part by the 111 Project under Grant B17040, and in part by the Fellowship of China Postdoctoral Science Foundation under Grant 2022M722945.

*Corresponding author
Email address: ckzhang@cug.edu.cn (Chuan-Ke Zhang)

to constructing appropriate Lyapunov-Krasovskii functionals (LKFs) and/or estimating their derivatives with conservatism-reduced inequalities. For instance, a standard LKF and the free-weighting matrices technique [21] are investigated to establish the LMIs-based stability criterion [7]. During the construction of the LKFs, relationships among different delays are considered while estimating integral terms with Jensen inequality [8, 22]. In [23], less conservative results are obtained by applying the Wirtinger-based integral inequality combined with the reciprocally convex approach [24]. The infinite-series-based inequality and the truncated second-order Bessel-Legendre (BL) inequality, which encompasses the Jensen inequality and the Wirtinger-based integral inequality, are used for estimating the derivatives tightly [25, 26]. Furthermore, in [27], less conservative stability criteria are derived based on the BL inequality together with the model reconstruction techniques, and comparative results are presented by using the linear operator inequality [28].

Currently, power grid online analysis has been widely used in dispatching control centers [29]. Otherwise, supervisory control and data acquisition (SCADA), state estimation, and contingency analysis are normally updated in an interval of minutes, which is not fast enough to recognize and anticipate system status if there is an emergency [30]. The above research methods pay many efforts into improving the calculation accuracy while ignoring the heavy computation burden in the stability analysis of complex power systems. This deficiency limits the applications to online analysis and real-time data processing and computation. Therefore, the methods in [31, 32] enhance the solvability of large-scale LMI-based conditions for analyzing the delayed LFC scheme by reducing the maximum order of LMI conditions [33] or cutting the decision variables based on the reconstructed LFC model [34]. The calculated upper bounds of time delays are decreased because more constraints are placed on the system model/stability criteria to reduce the computation burden. That is, the calculation efficiency is improved to meet the time demand of online stability analysis within the range of allowable accuracy reduction. However, these conservative conditions or results are unable to guide offline controller design with desired control performance, and the reliability of controller tuning is decreased. Overall, the existing studies put forward fixed stability conditions that cannot flexibly meet the demand of online stability analysis or offline controller design.

This paper investigates the delay-dependent stability analysis of the delayed LFC system by proposing novel demand-oriented methods. The accuracy and computation efficiency can be flexibly regulated for achieving both online stability analysis and offline controller design as demanded. Based on the time-domain method, variable LKFs are constructed by introducing multiple integral terms whose order is compatible with the tightly integral inequality used to bound the derivatives of the LKFs. Then, a new algorithm is designed. A threshold parameter is introduced to calculate the desired upper bounds of time delays and to meet the demand of computation efficiency for stability analysis. Case studies are carried out on the two-area LFC scheme and the IEEE 39-bus system to validate the effectiveness of the presented methods. The main contributions are summarized below.

- The proposed methods can realize the on-demand regulations of accuracy and computational efficiency, i.e., a small threshold parameter matches less conservative results but with more decision variables required in the LMIs to be resolved, and vice versa.

- The proposed methods combine well with the reconstructed model. Within the allowable range of accuracy reduction, this paper obviously improves the computation efficiency and prompts its application to online stability analysis. Whereas, the frequency-domain method has to calculate the large-scale characteristic equation with heavy computation burden.

- Presetting the zero threshold parameter leads to almost accurate results. In contrast, the previous time-domain methods inevitably introduce conservatism. Thus, when delay margins are adopted as an additional performance index for designing controllers offline, this paper achieves better robust performance than existing studies do.

The remaining parts of this paper are organized as follows. Section 2 presents the system model and the transformed one. Section 3 shows the proposed methods for stability analysis of the LFC system, including the novel asymptotical stability criteria and an algorithm. In Section 4, case studies are carried out to verify the effectiveness of the established stability criteria. In Section 5, conclusions are summarized.

2. Dynamic model of the multi-area LFC scheme

The dynamic model of the multi-area LFC schemes is given. Then, based on the model reconstruction technique [34], the original model is transformed into a coupled system consisting of a delay-related subsystem and a delay-free subsystem.

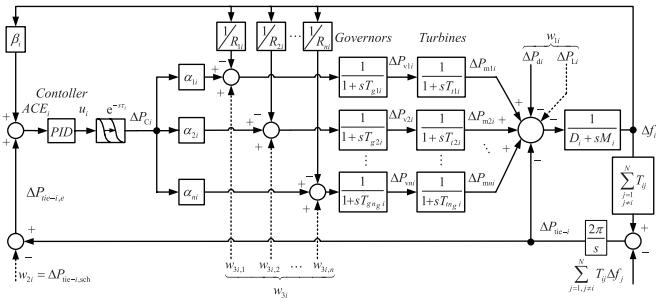

Figure 1: Structure of control area i (Traditional LFC: without dotted line connection; Deregulated LFC: with dotted line connection)

Figure 1 demonstrates the structure of area i in the multi-area LFC schemes, where n_g generators are assumed to be equipped and installed with non-reheat turbines. Exponential block $e^{-s\tau_i}$ shows delays arising in communication channels of area i. More notations employed in the ith area of the LFC system are explained in Table 1.

The ACE of area i is defined as

$$ACE_i = \beta_i \Delta f_i + \Delta P_{tie-i,e} \tag{1}$$

and a PID-type LFC controller is employed

$$u_i(t) = -K_{Pi} ACE_i - K_{Ii} \int ACE_i dt - K_{Di} \frac{dACE_i}{dt} \tag{2}$$

where K_{Pi}, K_{Ii} and K_{Di} are the proportional, integral and differential gains, respectively. Note that the following system model is established for the multi-area LFC scheme with N control areas. Therefore, there are N different time delays $(\tau_1, \tau_2, \dots \tau_N)$ included. Here, the closed-loop model of the traditional LFC scheme is recalled from [8].

$$\dot{x}(t) = Ax(t) + \sum_{i=1}^{N} \tilde{A}_{\mathrm{d}i} x(t-\tau_i) + B_{\mathrm{w}} \omega \tag{3}$$

where

$$x=[\bar{x}_1^T, \bar{x}_2^T, \dots, \bar{x}_N^T]^T, \ \ \bar{x}_i = [\hat{x}_i^T, \int y_i^T]^T, \ \ y_i = ACE_i$$

$$\hat{x}_i=\left[\Delta f_i, \Delta P_{tie-i,e}, \Delta P_{m1i}, \dots, \Delta P_{mn_gi}, \Delta P_{v1i}, \dots, \Delta P_{vn_gi}\right]^T$$

$$A = \begin{bmatrix} \bar{A}_{11} & \cdots & \bar{A}_{1N} \\ \vdots & \ddots & \vdots \\ \bar{A}_{N1} & \cdots & \bar{A}_{NN} \end{bmatrix}, \tilde{A}_{\mathrm{d}i} = \begin{bmatrix} 0_{(i-1)(2n_g+2)\times N(2n_g+2)} \\ \bar{A}_{\mathrm{d}i1} \ \ \bar{A}_{\mathrm{d}i2} \ \ \cdots \ \ \bar{A}_{\mathrm{d}iN} \\ 0_{(N-i)(2n_g+2)\times N(2n_g+2)} \end{bmatrix}$$

$$B_{\mathrm{w}} = \mathrm{diag}\{\bar{B}_{\mathrm{w}1}, \cdots, \bar{B}_{\mathrm{w}N}\}, \ \omega = \mathrm{diag}\{\omega_1, \cdots, \omega_N\}$$

$$\bar{A}_{\mathrm{d}ii} = -\bar{B}_i K_i \bar{C}_i, \ \bar{A}_{\mathrm{d}ij} = -\bar{B}_i K_i \bar{C}_{ij}, \ \bar{B}_{\mathrm{w}i} = \bar{F}_i - \bar{B}_i K_i \bar{D}_i$$

$$\bar{A}_{ii} = \begin{bmatrix} A_i & 0 \\ C_i & 0 \end{bmatrix}, \ \bar{A}_{ij} = \begin{bmatrix} A_{ij} & 0 \\ 0 & 0 \end{bmatrix}, \ \bar{B}_i = \begin{bmatrix} B_i \\ 0 \end{bmatrix}, \ \bar{F}_i = \begin{bmatrix} F_i \\ D_i \end{bmatrix}$$

$$\bar{C}_i = \begin{bmatrix} C_i & 0 \\ 0 & 1 \\ C_i A_i & 0 \end{bmatrix}, \bar{C}_{ij} = \begin{bmatrix} 0 & 0 \\ 0 & 0 \\ C_i A_{ij} & 0 \end{bmatrix}, \bar{D}_i = \begin{bmatrix} D_i \\ 0 \\ C_i F_i \end{bmatrix}$$

$$A_i = \begin{bmatrix} A_{11i} & A_{12i} & 0_{2\times n_g} \\ 0_{n_g\times 2} & A_{22i} & A_{23i} \\ A_{31i} & 0_{n_g\times n_g} & A_{33i} \end{bmatrix}, A_{ij} = \begin{bmatrix} 0 & 0 & 0_{1\times 2n_g} \\ -2\pi T_{ij} & 0 & 0_{1\times 2n_g} \\ 0_{2n_g\times 1} & 0_{2n_g\times 1} & 0_{2n_g\times 2n_g} \end{bmatrix}$$

$$A_{11i} = \begin{bmatrix} -\frac{D_i}{M_i} & -\frac{1}{M_i} \\ 2\pi \sum_{j=1, j\neq i}^{N} T_{ij} & 0 \end{bmatrix}, A_{12i} = \begin{bmatrix} \frac{1}{M_i} & \cdots & \frac{1}{M_i} \\ 0 & \cdots & 0 \end{bmatrix}$$

$$A_{22i} = -A_{23i} = -\mathrm{diag}\left\{\frac{1}{T_{t1i}}, \cdots, \frac{1}{T_{tn_gi}}\right\}$$

$$A_{31i} = -\begin{bmatrix} \frac{1}{R_{1i}T_{t1i}} & \cdots & \frac{1}{R_{n_gi}T_{tn_gi}} \\ 0 & \cdots & 0 \end{bmatrix}^T$$

$$A_{33i} = -\mathrm{diag}\left\{\frac{1}{T_{g1i}}, \cdots, \frac{1}{T_{gn_gi}}\right\}, \ \ K_i = [K_{Pi}, K_{Ii}, K_{Di}]$$

$$B_i = \begin{bmatrix} 0_{2\times 1} \\ 0_{n_g\times 1} \\ B_{3i} \end{bmatrix}, B_{3i} = \left[\frac{\alpha_{1i}}{T_{g1i}}, \cdots, \frac{\alpha_{n_gi}}{T_{gn_gi}}\right]^T, F_i = \begin{bmatrix} \frac{-1}{M_i} & 0 & 0 \\ 0 & -2\pi & 0 \end{bmatrix}$$

$$D_i = [0, 0], \ \ C_i = \left[\beta_i, 1, 0_{1\times 2n_g}\right], \ \ \beta_i = \sum_{j=1}^{n_g} \frac{1}{R_{ji}} + D_i.$$

The model of the deregulated multi-area LFC scheme is established while considering the dotted line in Figure 1. Moreover, notations F_i and D_i need to be redefined as $F_i = \begin{bmatrix} \frac{-1}{M_i} & 0 & 0_{1\times n_g} \\ 0_{(1+n_g)\times 1} & 0_{(1+n_g)\times 1} & 0_{(1+n_g)\times n_g} \\ 0_{n_g\times 1} & 0_{n_g\times 1} & -A_{33i} \end{bmatrix}$ and $D_i = [0, -1, 0_{1\times n_g}]$, respectively.

Table 1: Notations Illustrations

Δf_i	Deviation of frequency
$\Delta P_{tie-i,e}$	Deviation of tie-line power exchange
$\Delta P_{\mathrm{m}n_gi}$	Deviation of generator mechanical output
$\Delta P_{\mathrm{v}n_gi}$	Deviation of valve position
$\Delta P_{\mathrm{d}i}$	Traditional: load; Deregulated: un-contracted demand
$\Delta P_{\mathrm{L}i}$	Contracted demand
$\Delta P_{\mathrm{tie}-i,sch}$	Scheduled tie-line power exchange
M_i	Moment of inertia of generator unit
D_i	Generator unit damping coefficient
T_{gn_gi}	Time constant of non-reheat turbine speed governor
T_{tn_gi}	Time constant of non-reheat turbine
R_{n_gi}	Speed drop
T_{ij}	Tie-line synchronizing coefficient between area i and j
β_i	Frequency bias factor
α_{n_gi}	Ramp rate factor

For analyzing the asymptotical stability of (3), we consider the following disturbance-free model

$$\dot{x}(t) = \sum_{i=0}^{N} A_i x(t-\tau_i) \tag{4}$$

where $A_0 = A$ and $A_i \in \{\tilde{A}_{\mathrm{d}1}, \tilde{A}_{\mathrm{d}2}, \dots, \tilde{A}_{\mathrm{d}N}\}$ are obtained by reordering the time delays with $0 = \tau_0 \leq \tau_1 \leq \dots \leq \tau_N$.

The closed-loop LFC scheme has a few delay-related states and coefficient matrices $A_i, i \in \mathbb{N}$ are sparse. Inspired by [31], the state variables selected for area i have the following relationships:

$$\begin{aligned} \Delta \dot{f}_i(t) &= \lambda(\Delta P_{m\kappa i}(t), \Delta P_{\mathrm{d}i}(t), \Delta P_{tie-i,e}(t)) \\ \Delta \dot{P}_{tie-i,e}(t) &= h(\Delta f_i(t), \Delta f_j(t)) \\ \Delta \dot{P}_{m\kappa i}(t) &= g(\Delta P_{m\kappa i}(t), \Delta P_{v\kappa i}(t)) \\ \Delta \dot{P}_{v\kappa i}(t) &= f(\Delta f_i(t), \Delta P_{v\kappa i}(t)) + \chi(\Delta f_i(t-\tau_i), \Delta P_{tie-i,e}(t-\tau_i)) \end{aligned} \tag{5}$$

where $\kappa = 1, 2, \dots, n_g$, and $\lambda(\cdot), h(\cdot), g(\cdot), f(\cdot)$ and $\chi(\cdot)$ are appropriate functions developed based on the transfer functions in Figure 1. In area i, only state variables $\Delta \dot{P}_{v\kappa i}(t)$ are influenced by the delayed states directly, which is also the case for other control areas. Therefore, variables $\Delta \dot{P}_{v\kappa i}(t), \kappa = 1, 2, \dots, n, i = 1, 2, \dots, N$ are separated from state vector x and placed in $x_2 \in R^{n_2}$. Meanwhile, $x_1 \in R^{n_1}$ consists of the other state variables included in x. By completing elementary row operation on system (4), it is derived that

$$\begin{bmatrix} \dot{x}_1(t) \\ \dot{x}_2(t) \end{bmatrix} = \begin{bmatrix} A_{11} & A_{12} \\ A_{21} & A_{22} \end{bmatrix} \begin{bmatrix} x_1(t) \\ x_2(t) \end{bmatrix} + \sum_{j=1}^{N} \begin{bmatrix} 0 & 0 \\ A_{\mathrm{d}j} & 0 \end{bmatrix} \begin{bmatrix} x_1(t-\tau_j) \\ x_2(t-\tau_j) \end{bmatrix} \tag{6}$$

where $x_1 \in R^{n_1}$ includes delayed states, $x_2 \in R^{n_2}$ donates other states.

When the nominal power system is considered with time-varying delays, to calculate the delay margins conveniently, all regions are assumed to have same time-varying delays [25, 26], satisfying following conditions

$$0 \leq d(t) \leq h, \dot{d}(t) \leq \mu \tag{7}$$

where h and μ are the upper bound and delay variation bound of the time-varying delay, respectively.

Therefore, model (6) turns into the following equation

$$\begin{bmatrix} \dot{x}_1(t) \\ \dot{x}_2(t) \end{bmatrix} = \begin{bmatrix} A_{11} & A_{12} \\ A_{21} & A_{22} \end{bmatrix} \begin{bmatrix} x_1(t) \\ x_2(t) \end{bmatrix} + \begin{bmatrix} 0 & 0 \\ \sum_{j=1}^{N} A_{\mathrm{d}j} & 0 \end{bmatrix} \begin{bmatrix} x_1(t-d(t)) \\ x_2(t-d(t)) \end{bmatrix} \tag{8}$$

3. Delay-dependent Stability Analysis with Adjustable Accuracy and Computation efficiency

This section presents novel methods for investigating the stability analysis of the delayed LFC system (6), whose accuracy and computation efficiency can be regulated as required.

3.1. New stability condition

For developing the stability criteria, an integral inequality is recalled in Lemma 1.

Lemma 1. *[36] For a matrix $R > 0$ and a differentiable function $\{x(u), u\in[a,b]\}$, the following inequality holds*

$$\int_a^b \dot{x}^T(\alpha)R\dot{x}(\alpha)d\alpha \geq \sum_{l=0}^{n}\frac{\gamma_l}{b-a}\Omega_l^T(a,b)R\Omega_l(a,b) \tag{9}$$

where

$$\Omega_l(a,b)=\begin{cases}x(b)-x(a), & l=0\\ \sum\limits_{k=0}^{l}c_{k,l}x(b)-c_{0,l}x(a)-\sum\limits_{k=1}^{l}\frac{c_{k,l}k!}{(b-a)^k}\mathscr{I}^k_{(a,b)}x(t), & l\in\mathbb{N}^+\end{cases}$$

$$\gamma_l=\left(\sum_{k=0}^{l}\frac{c_{k,l}}{l+k+1}\right)^{-1}$$

$$c_{k,l}=\begin{cases}1, & k=l,\ l\geq 0\\ -\sum\limits_{v=k}^{l-1}\frac{\sum_{j=0}^{v}\frac{c_{j,v}}{l+j+1}}{\sum_{j=0}^{v}\frac{c_{j,v}}{v+j+1}}c_{k,v}, & k=0,1,\ldots,l-1,\ l\geq 1\end{cases}$$

$$\mathscr{I}^{\sigma}_{(a,b)}x(t)=\begin{cases}\int_a^b x(s)ds, & \sigma=1\\ \int_a^b\int_{s_1}^b\cdots\int_{s_{\sigma-1}}^b x(s_\sigma)\,ds_\sigma\ldots ds_2ds_1, & \sigma\geq 2,\ \sigma\in\mathbb{N}^+\end{cases}$$

The following criteria are developed by constructing variable LKFs and using Lemma 1 to bound their derivative. Its accuracy and calculation burden can be adjusted via an integer.

Theorem 1. *For given scalars $n\in\mathbb{N}$ and $\tau_i, i\in\mathbb{N}$ satisfying (4), system (6) is globally asymptotically stable, if there exist matrices $P, Q_j > 0, R_j > 0, j\in\mathbb{N}^+$ such that the following LMI holds*

$$\Xi=\Psi_aP\Psi_b^T+\Psi_bP\Psi_a^T+\sum_{j=1}^{N}\Upsilon_j<0 \tag{10}$$

where

$$\Psi_a=\begin{cases}\left[e_1^T,e_m^T\right], & n=0\\ \left[e_1^T,e_m^T,E_1^T,\ldots,E_N^T\right], & n\in\mathbb{N}^+\end{cases}$$

$$\Psi_b=\begin{cases}\left[e_{d1}^T,e_{dm}^T\right], & n=0\\ \left[e_{d1}^T,e_{dm}^T,E_{d1}^T,\ldots,E_{dN}^T\right], & n\in\mathbb{N}^+\end{cases}$$

$$e_{d1}=A_{11}e_1+A_{12}e_m$$

$$e_{dm}=A_{21}e_1+A_{22}e_m+\sum_{j=1}^{N}A_{\mathrm{dj}}e_{j+1}$$

$$E_j=\left[(b_j-a_j)e_{\ell_j}^T,\ldots,(b_j-a_j)^ne_{\ell_j}^T\right]$$

$$E_{dj}=\left[(e_j-e_{j+1})^T,(b_j-a_j)(e_j-e_{\ell_j})^T,\right.$$
$$\left.\ldots,(b_j-a_j)^{n-1}\left(\frac{1}{(n-1)!}e_j-e_{\ell_j-1}\right)^T\right]$$

$$\Upsilon_j=e_j^TQ_je_j-e_{j+1}^TQ_je_{j+1}+(\tau_j-\tau_{j-1})^2e_{d1}^TR_je_{d1}-\sum_{l=0}^{n}\gamma_l\Omega_{l,j}^TR_j\Omega_{l,j}$$

$$\Omega_{l,j}=\begin{cases}e_j-e_{j+1}, & l=0\\ \sum\limits_{k=0}^{l}c_{k,l}e_j-c_{0,l}e_{j+1}-\sum\limits_{k=1}^{l}c_{k,l}k!e_{lj+k}, & l=1,2,\ldots,n\end{cases}$$

$$e_q=\left[0_{n_1\times(q-1)n_1},I_{n_1\times n_1},0_{n_1\times(\ell_N-q)n_1},0_{n_1\times n_2}\right],\ q=1,2,\ldots,\ell_N$$

$$e_m=\left[0_{n_2\times\ell_Nn_1},I_{n_2\times n_2}\right]$$

$$\ell_j=\tilde{\ell}_j+n-1,\ \ \tilde{\ell}_j=N+2+(j-1)n,$$

$$a_j=t-\tau_j,\ \ b_j=t-\tau_{j-1}.$$

and $c_{k,l}$ is defined in (9).

Proof. The following variable LKF is constructed

$$V(t)=\zeta_n^T(t)P\zeta_n(t)+\sum_{j=1}^{N}\int_{a_j}^{b_j}x_1^T(s)Q_jx_1(s)ds+\sum_{j=1}^{N}\left(b_j-a_j\right)\int_{a_j}^{b_j}\int_{\theta}^{t}\dot{x}_1^T(s)R_j\dot{x}_1(s)dsd\theta \tag{11}$$

where

$$\zeta_n(t)=\begin{cases}\left[x_1^T(t),x_2^T(t)\right]^T, & n=0\\ \left[x_1^T(t),x_2^T(t),\mathscr{I}^1_{(a_1,b_1)}x_1^T(t),\ldots,\mathscr{I}^n_{(a_1,b_1)}x_1^T(t),\right.\\ \left.\ldots,\mathscr{I}^1_{(a_N,b_N)}x_1^T(t)\ldots,\mathscr{I}^n_{(a_N,b_N)}x_1^T(t)\right]^T, & n\in\mathbb{N}^+\end{cases}$$

and $P, Q_j > 0, R_j > 0, j\in\mathbb{N}^+$ remain to be determined.

Calculate the derivative of LKF (11) along (6). Then, bounding integral term $-\int_{a_j}^{b_j}\dot{x}_1^T(s)R_j\dot{x}_1(s)ds$ with Lemma 1 yields

$$\dot{V}(t)\leq\xi_n^T(t)\,\Xi\,\xi_n(t) \tag{12}$$

with

$$\xi_n(t)=\begin{cases}\left[x_1^T(t),x_1^T(a_1),\ldots,x_1^T(a_N),x_2^T(t)\right]^T, & n=0\\ \left[x_1^T(t),x_1^T(a_1),\ldots,x_1^T(a_N),\frac{1}{b_1-a_1}\mathscr{I}^1_{(a_1,b_1)}x_1^T(t),\right.\\ \ldots,\frac{1}{(b_1-a_1)^n}\mathscr{I}^n_{(a_1,b_1)}x_1^T(t),\ldots,\frac{1}{b_N-a_N}\mathscr{I}^1_{(a_N,b_N)}x_1^T(t),\\ \left.\ldots,\frac{1}{(b_N-a_N)^n}\mathscr{I}^n_{(a_N,b_N)}x_1^T(t),x_2^T(t)\right]^T, & n\in\mathbb{N}^+\end{cases}.$$

It can be found that the holding of LMI-based condition in Theorem 1 leads to $\dot{V}(t)\leq-\varepsilon\|x(t)\|^2$ for a sufficient small scalar $\varepsilon>0$, which ensures the asymptotical stability of (6).

Remark 1. *Augmenting (11) introduces multiple integral terms that fully benefit from inequality (9), e.g., the extension consists of incorporating $\mathscr{I}^n_{(a_N,b_N)}x_1^T(t)$, which appears spontaneously in (9). Then, the obtained stability criterion, Theorem 1, forms a set of LMI conditions with n adjusting its conservatism and calculation burden. By increasing n, it is expected to achieve many numerical improvements in calculating delay margins. Hence, Theorem 1 contains the existing results [27, 34]. Moreover, setting a relatively large n potentially obtains results that approximate the accurate value calculated by the frequency-domain method [15]. In Section III.B, an algorithm will be proposed to meet special requirements on computational accuracy for offline controller design or calculation speed for online stability analysis.*

For investigating the delay-dependent stability analysis of the LFC scheme with time-varying delays, Theorem 2 is presented.

Theorem 2. *For given scalars $n \in \mathbb{N}^+$, h and μ, system (8) is globally asymptotically stable, if there exist matrices $\tilde{P}, \tilde{Q}_1 > 0, \tilde{Q}_2 > 0, \tilde{R}_1 > 0$, and any matrix V such that the following LMI holds*

$$\tilde{\Xi} = \phi_a \tilde{P} \phi_b^T + \phi_b \tilde{P} \phi_a^T + \tilde{\Upsilon} < 0, \quad S > 0 \tag{13}$$

where

$$\tilde{\Upsilon} = \tilde{e}_1^T(\tilde{Q}_1+\tilde{Q}_2)\tilde{e}_1-(1-\mu)\tilde{e}_2^T\tilde{Q}_2\tilde{e}_2-\tilde{e}_3^T\tilde{Q}_2\tilde{e}_3+h^2\tilde{e}_{d1}^T\tilde{R}_1\tilde{e}_{d1}-E_nSE_n^T$$

$$\phi_a = \left[\tilde{e}_1^T, \tilde{e}_m^T, d(t)\tilde{e}_4^T, (h-d(t)\tilde{e}_5^T, \ldots, d(t)\tilde{e}_{2n+2}^T, (h-d(t)\tilde{e}_{2n+3}^T\right]$$

$$\Psi_b = \Big[\tilde{e}_{d1}^T, \tilde{e}_{dm}^T, \tilde{e}_1^T - (1-\mu)\tilde{e}_2^T, (1-\mu)\tilde{e}_2^T - \tilde{e}_3^T, \ldots, \frac{\tilde{e}_1^T}{(n-1)!} - (1-\mu)\tilde{e}_{2n}^T - (n-1)\mu\tilde{e}_{2n+2}^T, \frac{(1-\mu)\tilde{e}_2^T}{(n-1)!} - \tilde{e}_{2n+1}^T + (n-1)\mu\tilde{e}_{2n+3}^T\Big]$$

$$\tilde{e}_{d1} = A_{11}\tilde{e}_1 + A_{12}\tilde{e}_m$$

$$\tilde{e}_{dm} = A_{21}\tilde{e}_1 + A_{22}\tilde{e}_m + \sum_{j=1}^{N} A_{\mathrm{d}j}\tilde{e}_2$$

$$E_n = \left[E_{q0}^T, E_{q1}^T, \ldots, E_{qn}^T, E_{r0}^T, E_{r1}^T, \ldots, E_{rn}^T\right]$$

$$S = \Big\{\mathrm{diag}\{\rho_0\tilde{R}_1, \rho_1\tilde{R}_1, \ldots, \rho_n\tilde{R}_1\}\ V;\ V^T\ \mathrm{diag}\{\rho_0\tilde{R}_1, \rho_1\tilde{R}_1, \ldots, \rho_n\tilde{R}_1\}\Big\}$$

$$E_{ql} = \begin{cases} \tilde{e}_1 - \tilde{e}_2, & l=0 \\ \tilde{e}_1 - \frac{c_{0,l}\gamma_l}{\rho_l}\tilde{e}_2 - \frac{\gamma_l}{\rho_l}\sum_{k=1}^{l} c_{k,l}k!\tilde{e}_{2k+2}, & l=1,\ldots,n \end{cases}$$

$$E_{rl} = \begin{cases} \tilde{e}_2 - \tilde{e}_3, & l=0 \\ \tilde{e}_2 - \frac{c_{0,l}\gamma_l}{\rho_l}\tilde{e}_3 - \frac{\gamma_l}{\rho_l}\sum_{k=1}^{l} c_{k,l}k!\tilde{e}_{2k+3}, & l=1,\ldots,n \end{cases}$$

$$\rho_l = \begin{cases} 1, & l=0 \\ \gamma_l\left(\sum_{k=0}^{l} c_{k,l}\right)^2, & l=1,\ldots,n \end{cases}$$

$$\tilde{e}_r = [0_{n_1\times(r-1)n_1}, I_{n_1\times n_1}, 0_{n_1\times(2n+3-r)n_1}, 0_{n_1\times n_2}]$$

$$\tilde{e}_m = [0_{n_2\times(2n+3)n_1}, I_{n_2\times n_2}], r = 1, 2, \ldots, 2n+3.$$

Proof. Construct the following variable LKF

$$\tilde{V}(t) = \eta_n^T(t)\tilde{P}\eta_n(t) + \int_{t-d(t)}^{t} x_1^T(s)\tilde{Q}_1 x_1(s)ds + \int_{t-h}^{t} x_1^T(s)\tilde{Q}_2 x_1(s)ds + h\int_{-h}^{0}\int_{t+\theta}^{t} \dot{x}_1^T(s)\tilde{R}_1\dot{x}_1(s)dsd\theta \tag{14}$$

where

$$\eta_n(t) = \Big[x_1^T(t), x_2^T(t), \mathscr{I}^1_{(t-d(t),t)}x_1^T(t), \mathscr{I}^1_{(t-h,t-d(t))}x_1^T(t), \ldots, \frac{1}{d^{n-1}(t)}\mathscr{I}^n_{(t-d(t),t)}x_1^T(t), \frac{1}{(h-d(t))^{n-1}}\mathscr{I}^n_{(t-h,t-d(t))}x_1^T(t)\Big]^T$$

and $\tilde{P}, \tilde{Q}_1 > 0, \tilde{Q}_2 > 0$ and $\tilde{R}_1 > 0$ remain to be determined.

Calculating the derivative of LKF (14) and estimating its integral term with Lemma 1 together with the reciprocally convex approach yield

$$\dot{\tilde{V}}(t) \le \varsigma_n^T(t)\,\tilde{\Xi}\,\varsigma_n(t) \tag{15}$$

with

$$\varsigma_n(t) = \Big[x_1^T(t), x_1^T(t-d(t)), x_1^T(t-h), \frac{1}{d(t)}\mathscr{I}^1_{(t-d(t),t)}x_1^T(t), \frac{1}{h-d(t)}\mathscr{I}^1_{(t-h,t-d(t))}x_1^T(t), \ldots, \frac{1}{d^n(t)}\mathscr{I}^n_{(t-d(t),t)}x_1^T(t), \frac{1}{(h-d(t))^n}\mathscr{I}^n_{(t-h,t-d(t))}x_1^T(t), x_2^T(t)\Big]^T$$

and $\tilde{\Xi}$ defined in (13).

Remark 2. *In the proof of Theorems 1 and 2, there exist similarities between LKFs (11) and (14). To achieve the adjustability of derived criterion, both augmented terms $\zeta_n(t)$ in (11) and $\eta_n(t)$ in (14) introduce multiple integral terms, coordinating with n-order bounded integral inequality (9). Theorem 1 is used to investigate the delayed LFC scheme, and control areas have different constant delays satisfying (4). Therefore, for constructing LKF (11), the relationships between different delays are considered, leading to the less conservative stability criterion. Theorem 2 is established for the delayed power system with same time-varying delays $d(t)$ assumed in all control areas. Hence, we take full advantage of the time delay information during the construction of (14), and thus, delay variation bound μ is introduced into the derived condition.*

Remark 3. *Since our method can combine the reconstructed models (6) and (8) to construct LKFs (11) and (14), respectively, the computation complexity is decreased for delay-dependent stability analysis of large-scale power systems. By contrast, when the case of constant delays is discussed, the frequency-domain method [15] has to calculate the high-order characteristic equation based on the original large-scale power system. When the LFC system with time-varying delays is studied, Theorem 2 releases the computation burden of the criteria in [25, 26] by introducing a variable integer to change the constructed LKFs and estimation method flexibly.*

3.2. New algorithm

The following algorithm is designed to realize the demand-oriented regulation scheme, where τ_n^v shows the delay margin by solving the presented criteria with n. Define increment index ($\delta_v(\%)$) for delay margins calculated by the presented criteria where degree n increases to $n+1$. Additionally, a threshold parameter ρ is introduced.

$$\delta_v(\%) = \frac{\tau_{n+1}^v - \tau_n^v}{\tau_{n+1}^v}. \tag{16}$$

For investigating online stability analysis of system operation status, Algorithm 1 runs online. The computation speed and time consumption need to be considered preferentially within the range of accuracy reduction. Thus, if the results with some conservatism are acceptable for online stability analysis, we can set a relatively large ρ in Algorithm 1. A smaller n is required in Theorems 1 and 2 while guaranteeing their computation efficiency and ensuring the applications to online evaluation of system operation status.

On the other hand, setting relatively small ρ helps compute upper bounds with less conservatism, and a large integer n to-

gether with more decision variables is often demanded in Theorems 1 and 2. Especially, we can obtain the almost accurate delay margins by setting threshold parameter $\rho = 0$. This case is valuable for designing controllers with desired control performance because the almost accurate delay margin is employed as an additional performance index to guide the controller design. For controller design, Algorithm 1 runs offline regardless of the increased computation burden. Therefore, Algorithm 1 combined with Theorems 1 and 2 realizes the demand-oriented regulation scheme.

Algorithm 1: Demand-oriented regulation scheme

Step 1: Preset a search interval $[\tau_s, \tau_e]$, an accuracy requirement τ_{ac}, a threshold parameter ρ, and $n = 0$;

Step 2: Check the feasibility of LMI (10) (or LMI (13)) for given $\tau_{set} = (\tau_s + \tau_e)/2$.
If (10) (or (13)) is feasible, set $\tau_s = \tau_{set}$; else, set $\tau_e = \tau_{set}$.

Step 3: If $\tau_e - \tau_s \leq \tau_{ac}$, obtain delay margin $\tau_n^v = \tau_s$;
else, repeat **Step 2**.

Step 4: Increase $n = n + 1$ for LMI (10) (or LMI (13)) .
Repeat **Step 2** and **Step 3** to obtain delay margin τ_n^v.

Step 5: If $(\tau_n^v - \tau_{n-1}^v)/\tau_n^v \geq \rho$, repeat **Step 4**;
else, output τ_n^v and n.

3.3. Summary of analysis steps

The steps of implementing the proposed approach can be briefly summarized as follows.

Step1. A reconstructed model is presented based on the original dynamic model of the closed-loop LFC schemes, as shown in Section II.

Step2. An algorithm is proposed to flexibly regulate the computation accuracy and efficiency of determining the delay margins by presetting a threshold parameter ρ and adjusting degree n.

Step3. The delay margins are calculated with respect to various PID gains, polar coordinate point θ, and degree n. The SDPT3 solver in MATLAB is used to check the feasibility of the derived criterion.

Step4. By making comparisons with the existing frequency-domain method, the calculation efficiency of the proposed time-domain method is verified.

Step5. Simulations are carried out to show the effectiveness of obtained theoretical results in stability analysis and controller design.

4. Case studies

Case studies are carried out on the traditional two-area LFC scheme with constant delays, deregulated two-area LFC scheme with time-varying delays, and IEEE 39-bus system with 10 generator units. The parameters used in case studies are given in Appendix I where Tables 10, 11 and 12 [8, 35]. Same computational environments are utilized, e.g., a Win 10 PC equipped with an Intel i5 CPU, an 8GB RAM, and a 64-bit operation system, and the same presets of the calculation procedure. The approaches are implemented on the MATLAB 2018b, and the SDPT3 solver in the YALMIP toolbox is to check the feasibility of the LMI-based consdition.

4.1. Calculation accuracy verifications

This section verifies that we can regulate n in Theorem 1 and 2 to change its conservatism flexibly. Setting Theorems 1 and 2 with a large n realizes the less conservative results, even the exact ones. Based on the two-area LFC model with different PID gains, how to determine the value of n for Theorem 1 is explained through the proposed algorithm. Moreover, based on the IEEE 39-bus system, it is shown that the results obtained with the proposed approach, are consistent with the actual power systems with model complexities and nonlinearities.

4.1.1. Two-area LFC schemes with constant delays

For integer $n \in [0, 3]$, Theorem 1 includes four stability criteria. The controller gain is assumed to be $K = [0.4\ 0.2\ 0]$. The calculated delay margins based on each criterion are tabulated in Table 2, where $\tau_n^v = \sqrt{\tau_1^2 + \tau_2^2}$ represents the magnitude of τ_1 and τ_2 and $\theta = \tan^{-1}(\tau_1/\tau_2)$, $\theta \in [0°, 90°]$. Figure 2 is given to show these results clearly. Meanwhile, the accurate results obtained by the frequency-domain method [15] are introduced as the benchmark.

Table 2: Delay Margins of Two-Area LFC Scheme with respect to n

	θ										
τ_n^v(s)	0°	10°	20°	30°	40°	45°	50°	60°	70°	80°	90°
$n = 0$	4.58	4.22	4.35	4.68	5.01	4.86	4.42	3.99	3.80	3.87	4.52
$n = 1$	7.13	7.58	8.15	9.29	11.10	8.63	10.96	9.00	7.86	7.40	6.98
$n = 2$	8.51	8.66	9.08	9.86	11.15	11.03	11.01	9.74	8.97	8.56	8.41
$n = 3$	8.54	8.67	9.09	9.86	11.15	11.93	11.01	9.74	8.97	8.56	8.43
Exact [15]	8.55	8.67	9.11	9.86	11.15	11.95	11.01	9.74	8.97	8.56	8.43

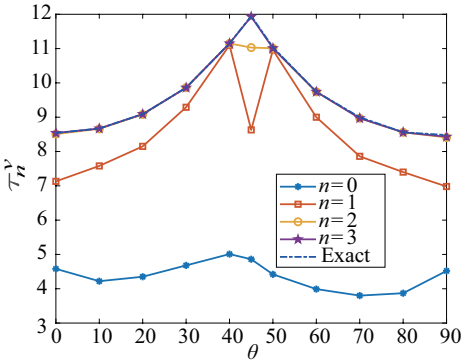

Figure 2: The estimated delay margins with respect to θ and n.

From Table 2 and Figure 2, the increased order of n lets the estimated delay margins approach the exact ones gradually, e.g., if $n = 3$, the purple line will coincide with the dotted line. For given $n = 3$, Theorem 1 can realize the almost same computational accuracy as the frequency-domain method. Note

that for given $n = 2$, Theorem 1 still computes the accurate delay upper bounds except for $\theta = 45°$.

Comparing with the result of the frequency-domain method (τ_e), the conservatism introduced by the proposed time-domain method is represented with relative error $\delta(\%)$. To clearly demonstrate the relationships among $\delta(\%)$, n, and θ, four typical cases are depicted in Figure 3.

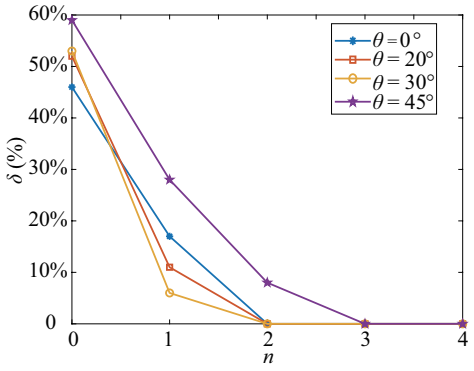

Figure 3: The introduced conservatism with respect to θ and n.

The purple line representing $\theta = 45°$ is always above the other three lines with $\theta \in [0°, 20°, 30°]$. When n is increased to 2, the following three lines decline to zero, and non-conservative results are obtained. Whereas, setting $\theta = 45°$ requires $n = 3$ to almost eliminate the conservatism introduced. It can be concluded that $\theta = 45°$ ($\tau_1 = \tau_2$) has the worst effect on determining the accurate delay margins, and therefore, the following parts start from $\theta = 45°$.

Here, we demonstrates how to determine the value of n for Theorem 1. Figure 4 displays the estimated upper bounds with respect to K_P and n with fixed $K_I = 0.15$. We can find that the lines for $n = 4$ and $n = 5$ coincide with each other (The increment index approximates zero) for all concerned values of K_P. Thus, for given $n = 4$, Theorem 1 enables the computation of non-conservative results. Actually, when $K_P \in [0, 0.1]$, five lines for $n \in [1, 2, 3, 4, 5]$ overlap each other, i.e., $n = 1$ is enough for obtaining the accurate delay upper bounds. When $K_P \in [0.1, 0.2]$, the line of $n = 2$ approaches the lines of $n \in [3, 4, 5]$ and obtains the stability criterion without conservatism. In addition, when $K_P \in [0.2, 0.4]$ and $K_P \in [0.4, 0.6]$, setting $n = 3$ and $n = 4$ for Theorem 1 can almost vanish its conservatism, respectively. It is obvious that the conservatism of delay margins varies with the different PID gains. However, the proposed method eliminates this bad effect, obtaining the delay upper bounds with almost consistent accuracy for any given PID gains.

After defining increment index $\delta_v(\%)$ and threshold parameter ρ for delay margins as shown in Algorithm 1, we realizes the special requirements on accuracy or calculation efficiency. Table 3 shows increment indices for delay margins with increased n under different PID controllers.

If $\rho = 2\%$ is desired, then, $n = 2$ is required for $K_P \in [0, 0.1]$; $n = 3$ is enough for $K_P = 0.2$; $n = 4$ is needed for $K_P \in [0.3, 0.4]$, and $n = 5$ is required for $K_P \in [0.5, 0.6]$. Presetting $\rho = 0\%$ leads to almost accurate results while demanding a

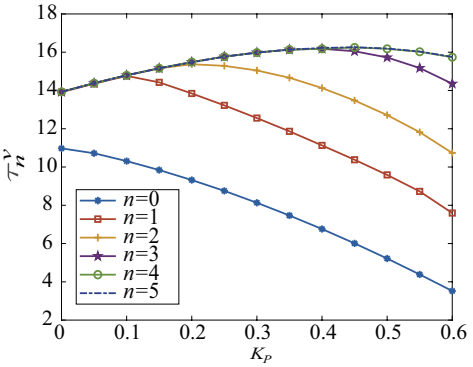

Figure 4: The estimated delay margins with respect to K_P and n ($K_I = 0.15$).

Table 3: Increment Indices of Delay Margins with Increased n under Different K_P Gains

n	$0 \to 1$	$1 \to 2$	$2 \to 3$	$3 \to 4$	$4 \to 5$
$K_P = 0$	21.06%	0.17%	0.00%	0.00%	0.00%
$K_P = 0.1$	30.19%	0.22%	0.00%	0.00%	0.00%
$K_P = 0.2$	32.74%	9.90%	0.76%	0.00%	0.00%
$K_P = 0.3$	35.23%	16.59%	5.82%	0.00%	0.00%
$K_P = 0.4$	39.24%	21.21%	12.65%	0.00%	0.00%
$K_P = 0.5$	45.52%	24.61%	19.16%	2.76%	0.00%
$K_P = 0.6$	53.70%	29.15%	25.28%	8.78%	0.00%

relatively large n and resulting in the increased scale of LMIs.

Additionally, Figure 5 shows the estimated delay margins with respect to $K_I \in [0.05, 0.6]$ and n with fixed $K_P = 0.4$. It can be seen that the lines for $n = 4$ and $n = 5$ coincide with each other for all concerned values of K_I. Thus, we can conclude that for given $n = 4$ in Theorem 1, the almost accurate delay margins can be computed. In detail, for $K_I \in [0.05, 0.1]$, $n = 4$ is required for approaching $n = 5$; for $K_I \in [0.1, 0.25]$, $n = 3$ is enough; for $K_I \in [0.25, 0.45]$, $n = 2$ derives the almost accurate upper bounds; for $K_I \in [0.45, 0.6]$, $n = 1$ leads to non-conservative criterion. Table 4 lists these results.

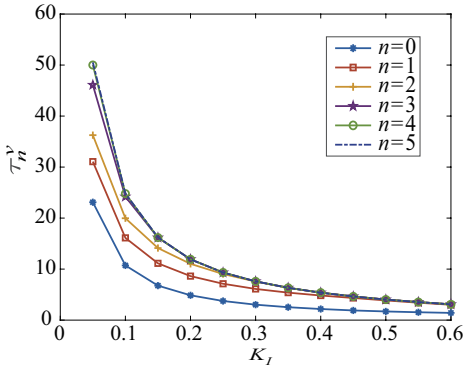

Figure 5: The estimated delay margins with respect to K_I and n ($K_P = 0.4$).

In this case, if we preset threshold parameter $\rho = 5\%$, $n = 2$ is required for $K_I \in [0.5, 0.6]$; $n = 3$ is enough for $K_I \in [0.3, 0.4]$, and $n = 4$ is needed for $K_I \in [0.1, 0.2]$. If $\rho = 2\%$, $n = 3$ is for $K_I \in [0.3, 0.6]$; $n = 4$ is for $K_I = 0.2$, and $n = 5$ is for $K_I = 0.1$. Moreover, setting $\delta_{vr} = 0\%$ will output the almost accurate results with a relatively big n, implying increased calculation burden. Here clarifies the flexible regulations on computational

accuracy or efficiency.

Table 4: Increment of Delay Margins with Increased n under Different K_I Gains

n	$0 \to 1$	$1 \to 2$	$2 \to 3$	$3 \to 4$	$4 \to 5$
$K_I = 0.1$	33.48%	19.30%	17.49%	2.37%	0.00%
$K_I = 0.2$	43.73%	21.76%	7.48%	0.00%	0.00%
$K_I = 0.3$	50.39%	19.30%	0.27%	0.00%	0.00%
$K_I = 0.4$	55.00%	10.32%	0.18%	0.00%	0.00%
$K_I = 0.5$	56.09%	4.20%	0.17%	0.00%	0.00%
$K_I = 0.6$	53.11%	2.74%	0.15%	0.00%	0.00%

4.1.2. IEEE 39-bus system

This case study has two objectives. First, when the increment index is zero as n is added by one in LMI (10), n is enough for (10) to obtain the almost accurate results. Then, the theoretical results investigated based on the time-domain method are consistent with the practical solutions of the real-world power system. Typical parameters for turbine-governor systems are $T_g = 0.08$ s, $T_t = 0.40$ s, and droop characteristic $R = 5\%$ p.u./rated power. For numerical tests, the actual values of T_g, T_t and R are randomly generated in the range of $1 \pm 10\%$ of the typical values.

Figure 7 shows the single-line diagram for the IEEE 39-bus system, including 10 synchronous generators, 19 loads, 34 transmission lines, and 12 transformers. Each generator is equipped with the excitation unit and power system stabilizer (PSS). System data and parameters of generators, transformers, and transmission lines are given in [35]. As shown in Figure 7, the three-area test case is obtained by dividing 10 generators into three control areas, i.e., machines G1 to G3, G4 to G7, and G8 to G10 are organized into areas 1, 2, and 3, respectively. It is assumed that in all control areas, all generators are equipped with the conventional PID-based secondary frequency control loops. In the performed application, the important inherent requirements and basic constrains, such as governor dead band (GDB) and generation rate constraint (GRC) imposed by physical system dynamics, are considered. Figure 6 describes diagrams of the GDB and GRC, in which the GRC is assumed to be ±0.1 pu/min, and the range of GDB is 0.036 HZ [5].

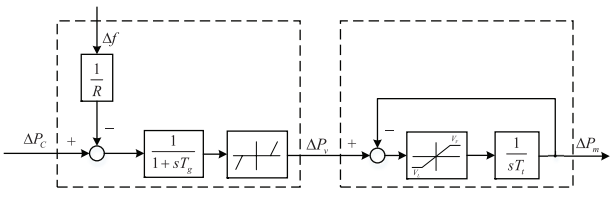

Figure 6: Structures of GDB and GRC in the LFC scheme.

This figure also describes the tie-lines between area 1 and area 3 (connecting buses 1-39 and 3-4), the tie-line between area 1 and area 2 (connecting bus 14-15), and the tie-line between area 2 and area 3 (connecting bus 16-17). Based on the parameters given in [35], the tie-line synchronizing torque coefficients of this three-area system can be calculated with $T_{12} = 0.4166$, $T_{13} = 1.3272$, and $T_{23} = 0.2959$.

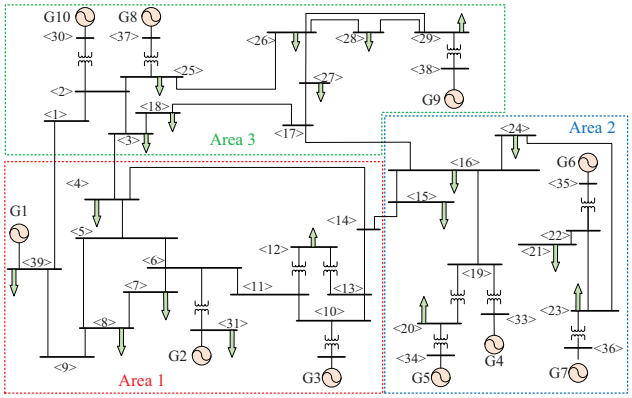

Figure 7: Structure of 10 units IEEE 39-bus system.

Delay margin $\tau = \sqrt{\tau_1^2 + \tau_2^2 + \tau_3^2}$ is calculated with respect to various PID controller gains and n. The results are listed in Table 5, where the increment indices for upper bounds are reflected with the increased n. As mentioned before, when the time delays in each area are equal, i.e., $\tau_1 = \tau_2 = \tau_3$, it is hard to decrease the conservatism introduced by using the time-domain method. Therefore, the three-area test case is studied with identical delays.

Table 5: Delay Margins and Increment Indices with Increased n under Different PID Controllers

K	n						
	0	1	2	3	$0 \to 1$	$1 \to 2$	$2 \to 3$
[0.1 0.15 0]	10.68	15.01	15.01	15.01	28.85%	0.00%	0.00%
[0.2 0.2 0]	6.61	11.78	11.81	11.81	43.89%	0.23%	0.00%
[0.3 0.2 0]	5.31	11.51	12.18	12.18	53.87%	5.54%	0.00%
[0.3 0.3 0]	3.18	7.51	7.84	7.84	57.72%	4.20%	0.00%
[0.4 0.15 0]	5.56	13.41	15.82	15.82	58.56%	15.21%	0.00%
[0.4 0.3 0]	2.18	6.55	7.98	7.98	66.76%	17.94%	0.00%
[0.2 0.2 0.05]	7.13	12.05	12.08	12.08	40.81%	0.21%	0.00%
[0.3 0.2 0.05]	5.80	11.98	12.54	12.54	51.55%	4.50%	0.00%
[0.3 0.2 0.1]	6.37	12.41	12.93	12.93	48.72%	4.03%	0.00%
[0.4 0.15 0.1]	**7.15**	**14.96**	**15.82**	15.82	52.20%	5.44%	0.00%

Based on this practical test system, it is clear that the computation accuracy of the derived criterion is highly related to PID gains. For instance, setting $n = 1$ in Theorem 1 derives the fixed criterion in [34]. In this case, when $K = [0.1\ 0.15\ 0]$, the delay margin is obtained as 15.01s with little conservatism. In contrast, for $K = [0.3\ 0.2\ 0]$, the calculated delay margin is 11.51s by the existing fixed criterion, and it is far less than the real value (12.18s), i.e., some conservative results are realized in [34]. The practical delayed LFC system aims to obtain the accurate delay margins for any system parameters. Thus, these results are employed to guide such effective controller design that eliminates the adverse influence of time delay on system frequency stability. Motivated by this, the adjustable Theorem 1 is proposed. When n increases from 2 to 3, increment index $\delta_v(\%)$ approximates zero, implying $n = 2$ is enough for obtaining the almost accurate delay margins. Based on Algorithm 1, we can conclude that the conservatism of obtained delay margins is minimized by choosing $n = 2$ in Theorem 1. Especially,

when K = [0.1 0.15 0], setting n = 1 leads to the desired result. The computation complexity is reduced timely with this flexible method. Hence, considering the IEEE 39-bus system, we show that the proposed method can achieve the delay margins with almost consistent accuracy for any considered controller gains.

For simulation verification, the case of K = [0.4 0.15 0.1] is selected, for which n = 2 ($\delta_v(\%)$ = 0) remains to be verified with non-conservative result for the practical IEEE 39-bus system. The base value for power is 100 MVA and for frequency it is 60 Hz. Assume that three step load disturbances are simultaneously applied to the three areas at start: 10% of total area load in area 1, 8% of total area load in area 2, and 5% of total area load in area 3 (ΔP_{d1} = 0.1 pu, ΔP_{d2} = 0.08 pu, and ΔP_{d3} = 0.05 pu). Following the step disturbances, the responses of area 2 are depicted in Figure 8.

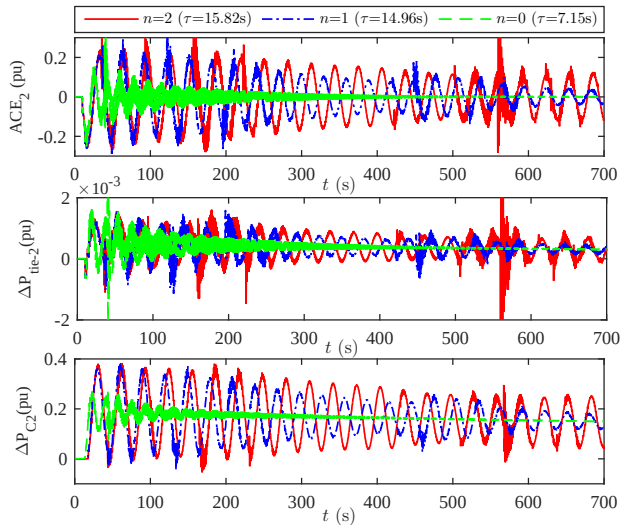

Figure 8: Responses of area 2 for the IEEE 39-bus system.

In Figure 8, when the delay margins obtained through Theorem 1 with n = 0 and n = 1 are introduced in the IEEE 39-bus system, the system responses are asymptotically stable. In contrast, setting n = 2 in Theorem 1 obtains τ = 15.82, which drives the critical stability of the IEEE 39-bus system. Thus, τ = 15.82 is the real upper bound for the IEEE 39-bus system equipped with K = [0.4 0.15 0.1], and n = 2 is enough for Theorem 1 to obtain the non-conservative result. This validates the effectiveness of the proposed method with a real-world power system.

4.1.3. *Two-area LFC schemes with time-varying delays*

By comparing with the existing results [25, 26], this case study aims to show the numerical improvements of Theorem 2. Results about the delay margins of the deregulated two-area LFC scheme equipped with different PID controllers are tabulated in Table 6 (μ = 0) and Table 7 (μ = 0.5), respectively. Due to the adjustability of Theorem 2, it calculates larger maximum allowable delay margins than the methods of [25] and [26] by regulating variable n. The effectiveness of the proposed criterion is validated in computation accuracy.

Table 6: Delay Margins of Deregulated LFC Scheme with Constant Delays (μ = 0)

K	[26]	[25]	Theorem 2			
			n = 1	n = 2	n = 3	n = 4
[0.00 0.10 0.00]	14.95	15.22	15.22	15.22	15.22	15.22
[0.00 0.20 0.00]	7.33	7.39	7.39	7.39	7.39	7.39
[0.00 0.40 0.00]	3.34	3.50	3.50	3.50	3.50	3.50
[0.05 0.20 0.00]	7.47	7.63	7.63	7.63	7.63	7.63
[0.20 0.20 0.00]	6.60	6.86	6.89	7.66	8.07	8.20
[0.05 0.20 0.02]	7.54	7.66	7.66	7.66	7.66	7.66
[0.05 0.20 0.05]	5.27	5.82	5.86	6.80	7.35	7.68

Table 7: Delay Margins of Deregulated LFC Scheme with Time-Varying Delays (μ = 0.5)

K	[26]	[25]	Theorem 2			
			n = 1	n = 2	n = 3	n = 4
[0.00 0.10 0.00]	13.41	13.47	13.74	18.42	19.84	20.18
[0.00 0.20 0.00]	6.49	6.54	6.86	9.25	9.98	10.17
[0.00 0.40 0.00]	3.02	3.08	3.39	4.61	4.99	5.12
[0.05 0.20 0.00]	6.68	6.72	6.90	9.25	10.00	10.21
[0.20 0.20 0.00]	0.21	0.22	0.43	0.77	0.89	0.95
[0.05 0.20 0.02]	6.54	6.71	6.82	9.16	9.91	10.17
[0.05 0.20 0.05]	0.27	0.32	0.38	0.67	0.82	0.84

4.2. *Controller design*

The proposed method is validated on calculating the almost accurate delay margins for any given PID controllers. In this section, how to guide the controller design with enhanced dynamic performance is discussed by using the obtained almost accurate delay margins as an additional performance index. It verifies that selecting controllers with the presented method has improved reasonability in comparison with fixed studies [34, 27]. Figure 9 shows delay margins (with respect to K_P, K_I = 0.15, K_D = 0) calculated with different methods.

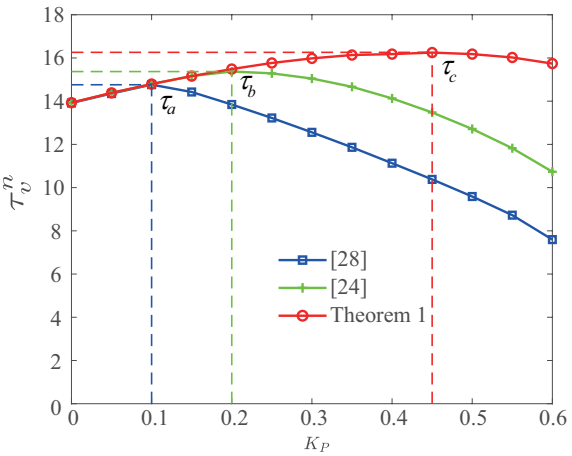

Figure 9: The estimated delay margins with different methods

As shown in Figure 9, when K_P increases from 0 to 0.6, the delay margin increases at first and then decreases. For guaranteeing the stability of power systems, choosing K_1 = [0.1 0.15 0] and K_2 = [0.2 0.15 0] obtains the maximal allowable delay upper bounds τ_a = 14.76s and τ_b = 15.37s, respectively. In contrast, through Theorem 1, the allowable maximum delay margin reaches τ_c = 16.26s with K_3 = [0.45 0.15 0].

Considering different scenarios, simulations are implemented to show superiorities of K_3 over K_1 and K_2 in the dynamic performances. Assume step loads of 0.05 pu and 0.08 pu appearing in areas 1 and 2, respectively. When time delays $\tau_v^n = 10$s, $\tau_v^n = 15$s, and $\tau_v^n = 16$s are introduced into the transmission channels, Figure 10 describes the responses of two-area LFC schemes with different controllers.

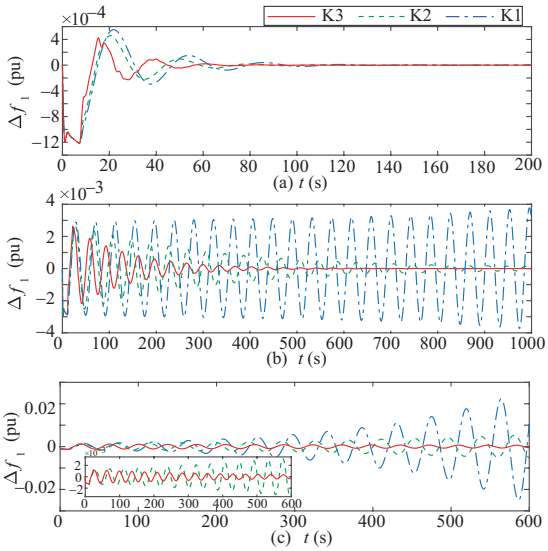

Figure 10: Responses of the two-area LFC scheme with different delays. (K_1 [34],K_2 [27], K_3 Theorem 1). (a) $\tau_v^n = 10$s, (b) $\tau_v^n = 15$s,(c) $\tau_v^n = 16$s.

In Figure 10, through the proposed method, the designed controller enhances the dynamic performance of the LFC scheme while keeping the best tolerance against time delays. Whereas, based on the existing methods, controllers K_1 or K_2 loses their capability. Therefore, conservative results cannot reflect right variation tendencies of delay margins against K_P, reducing dynamic performance of the designed controller.

Secondly, assume delay margin $\tau_n^v = 7s$. By setting $n = 4$ in Theorem 1, Figure 12 depicts stable regions of PI gains for two-area LFC schemes. The other two stable regions are given by [34, 27]. As shown in Figure 12, more freedom is allowed to design controllers by the proposed method, e.g., when $K_P = 0.7$ is fixed, we can choose $K_4 = [0.7\ 0.09\ 0]$ and $K_5 = [0.7\ 0.2\ 0]$ based on [34] and [27], respectively, but with Theorem 1, $K_6 = [0.7\ 0.28\ 0]$ is allowable.

When random time delays $(\tau_1, \tau_2 \in [0, 5]s)$ are introduced into in the two-area LFC system, Figure 11 records state responses of area 1. Controller K_6 enables systems to be stable with smaller frequency derivation and less settling time than K_4 and K_5 do. Therefore, we can design the LFC schemes with enhanced dynamic performance by using the almost accurate delay margins as an additional performance index in this paper.

4.3. Calculation efficiency verification

In this section, by comparing with the frequency-domain method [15] and existing time-domain methods [25, 26], the improved computational efficiency of this paper is validated for online stability analysis.

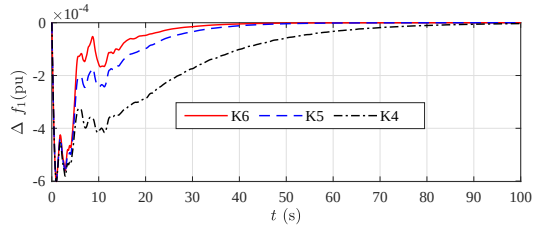

Figure 11: Responses of area 1 for the two-area LFC system with different controllers. (K_4 [34],K_5 [27], K_6 Theorem 1).

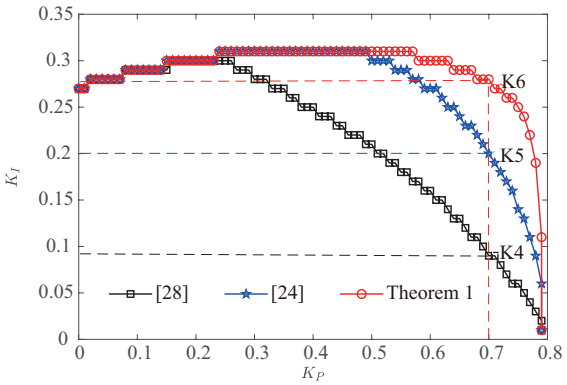

Figure 12: Stable regions of PI controllers under different methods.

Firstly, by comparing with the frequency-domain method, the calculation capability of Theorem 1 is verified. The number of decision variables (v_{T1}) and the maximum order (m_{T1}) of LMI (10) can be calculated as follows by referring to [8].

$$\begin{aligned} v_{T1} &= \frac{(Nnn_1+n_1+n_2)(Nnn_1+n_1+n_2+1)}{2} + Nn_1(n_1+1) \\ m_{T1} &= Nnn_1 + (N+1)n_1 + n_2 \end{aligned}$$

Table 9 shows detailed computational performances of the two methods by taking the IEEE 39-bus system as a numerical example. t_{T1} represents the calculation time spent on obtaining the delay margin by Theorem 1. "Na" denotes the method considered needs too much time to determine delay margins.

Table 9: Calculation Performance Comparisons on IEEE 39-Bus System with Constant Delays

	Theorem 1						Exact [15]
n	0	1	2	3	4	5	–
v_{T1}	622	1594	3142	5266	7966	11242	–
m_{T1}	52	76	100	124	148	172	–
t_{T1}(s)	2.0	5.8	21.5	58.6	139.6	301.1	Na

As we can see, the increased n enlarges the scale of LMI (10), and more CPU time is required for determining the upper bounds. Whereas, as LKF (11) is established by combining (6), it employs delayed part $x_1 \in R^{n_1}$ instead of the original system state $x \in R^{n_1+n_2}$ to deal with the delay information. Weighting matrices has decreased order, and thus, the computational burden of the LMI-based condition is obviously lowered. Thus, the method proposed is effective for the stability analysis of the IEEE 39-bus system. Whereas, the method in [15] has to compute the high-order characteristic equation based on the original system model, losing its capability of obtaining delay margin-

Table 8: Comparisons of Computational Performance on Deregulated Two-Area LFC Scheme with Time-Varying Delays

[26]			[25]			Theorem 2			Ratio					
v_{Ta}	m_{Ta}	t_{Ta}(s)	v_{Tb}	m_{Tb}	t_{Tb}(s)	v_{T2}	m_{T2}	t_{T2}(s)	$v_{\mathrm{T2}}/v_{\mathrm{Ta}}$	$m_{\mathrm{T2}}/m_{\mathrm{Ta}}$	$t_{\mathrm{T2}}/t_{\mathrm{Ta}}$	$v_{\mathrm{T2}}/v_{\mathrm{Tb}}$	$m_{\mathrm{T2}}/m_{\mathrm{Tb}}$	$t_{\mathrm{T2}}/t_{\mathrm{Tb}}$
13949	182	927.6	4615	104	99.3	955	49	4.4	6.9%	26.9%	0.5%	20.7%	47.1%	4.4%

s. Thus, the calculation efficiency of the proposed method is verified.

Secondly, to verify the calculation efficiency of Theorem 2, the number of decision variables and the maximum order of LMIs in Theorem 2 $(v_{\mathrm{T2}}, m_{\mathrm{T2}})$, Theorem 1 [25] $(v_{\mathrm{Ta}}, m_{\mathrm{Ta}})$, and Theorem 1 [26] $(v_{\mathrm{Tb}}, m_{\mathrm{Tb}})$ can be calculated with the following formulas.

$$
\begin{aligned}
v_{\mathrm{T2}} &= \frac{((2n+1)n_1 + n_2(2n+1)n_1 + n_2 + 1)}{2} + \frac{3n_1(n_1+1)}{2} + (n+)^2 n_1^2 \\
m_{\mathrm{T2}} &= (2n+3)n_1 + n_2 \\
v_{\mathrm{Ta}} &= 82n_1^2 + 82n_2^2 + 164n_1n_2 + 7n_1 + 7n_2 \\
m_{\mathrm{Ta}} &= 14n_1 + 14n_2 \\
v_{\mathrm{Tb}} &= 27n_1^2 + 27n_2^2 + 54n_1n_2 + 4n_1 + 4n_2 \\
m_{\mathrm{Tb}} &= 8n_1 + 8n_2
\end{aligned}
$$

When the deregulated two-area LFC scheme is considered, the numerical computation indices of different methods are given in Table 8. It is clear that, compared with the stability criteria in [25] and [26], our result significantly reduces the size of LMI-based condition together with decision variables. Thus, only 4.4% the computation time is required by Theorem 2 for calculating delay margins in comparison with Theorem 1 in [26]. By comparing Theorem 2 and Theorem 1 in [25], the percentage is decreased to 0.5%. Here verifies the computation efficiency of Theorem 2.

5. Conclusion

This paper has investigated the delay-dependent stability of the delayed cyber-physical power systems (DCPPS). Based on the time-domain method, a flexible regulation scheme has been presented by developing the stability criteria in terms of linear matrix inequality techniques (LMIs) and an algorithm. As the proposed method is adjustable in conservatism and calculation efficiency, the algorithm has been designed with a threshold parameter to calculate the desired upper bounds and meet the demand of computation efficiency.

Case studies have employed the two-area LFC schemes and the IEEE 39-bus system as test systems. It has been verified that the proposed method can realize the particular requirements in less conservative results or less computation complexity. Especially, presetting the proposed time-domain method with the zero threshold parameter reaches almost non-conservative delay margins. When the delay margin is employed as an additional index to guide controller design, such a method has been validated with more reliability and effectiveness. Moreover, within the allowable range of calculation accuracy reduction, the flexible regulation scheme has been validated in online stability analysis with the obviously increased computation capability compared to the frequency-domain method.

The proposed techniques are variable in terms of computational burden and accuracy. They can be extended to design event-triggered LFC schemes, which adaptively adjusts the threshold parameter of the event-triggered LFC scheme based on the variable bandwidth status and system output change. Thus, the communication burden is lessened while ensuring desired control performance. Additionally, the presented approaches are available for investigating the delay-dependent stability analysis of the delayed wide-area damping control systems (WADCs) to design reliable controllers. In the other hand, to improve the control performance and quality of the delayed LFC system, the accurate measurement, analysis, and prediction of network time delays are of great significance. This paper focuses on improving the analysis accuracy of the maximum allowable upper bounds while improving the reliability of the selected controller. Whereas, how to predict the time delay that the LFC system will suffer to adjust the controller gains remains to be investigated. Moreover, the derivation of theoretical bounds for the introduced conservatism for a certain class of systems still remains to be investigated in our future work.

Appendix I

Table 10 shows parameters for the traditional two-area LFC scheme with two generators. Table 11 presents parameter of the 10 units IEEE 39-bus system based three-area LFC scheme. The parameters of deregulated two-area LFC scheme are listed in Table 12 where each area has two generation companies and distribution companies.

Table 10: Parameters of Traditional Two-Area LFC Scheme

Area	T_t	T_g	R	D	β	M	α	T_{12}
1	0.30	0.10	0.05	1.00	21.0	10	1.00	0.1968
2	0.40	0.17	0.05	1.50	21.5	12	1.00	

Table 11: IEEE 39-Bus System based Three-Area LFC Scheme Parameters

Area		T_t	T_g	R	D	β	M	α	T_{ij}
1	G1	0.3742	0.0804	0.0471	0	21.2314	100	0.1703	$T_{12}=0.4166$
	G2	0.3888	0.0774	0.0541	0	18.4843	6.06	0.5523	$T_{13}=1.3272$
	G3	0.3645	0.0748	0.0518	0	19.3050	7.16	0.2774	
2	G4	0.3707	0.0759	0.0540	0	18.5185	5.72	0.2543	
	G5	0.3770	0.0729	0.0470	0	21.2766	5.20	0.3830	$T_{21}=0.4166$
	G6	0.4316	0.0791	0.0459	0	21.7865	6.96	0.3175	$T_{23}=0.2959$
	G7	0.3657	0.0722	0.0481	0	20.7900	5.28	0.0452	
3	G8	0.3665	0.0805	0.0484	0	20.6612	4.86	0.3981	$T_{31}=1.3272$
	G9	0.4222	0.0737	0.0479	0	20.8768	6.90	0.4398	$T_{32}=0.2959$
	G10	0.4324	0.0852	0.0525	0	19.0476	8.40	0.1621	

6. References

[1] H. Ye, K. Liu, Q. Mou, et al. "Modeling and formulation of delayed cyber-physical power system for small-signal stability analysis and control," *IEEE Trans. Power Syst.,* vol. 34, no. 3, pp. 2419-2432, 2019.

Table 12: Parameters of Deregulated Two-Area LFC Scheme

	($k-i$: k in area i)					Area	
	1-1	2-1	1-2	2-2		1	2
T_t	0.32	0.30	0.30	0.32	M	0.1667	0.2084
T_g	0.06	0.08	0.06	0.07	D	0.0084	0.0084
R	2.4	2.5	2.5	2.7	β	0.4250	0.3966
α	0.5	0.5	0.5	0.5	T_{12}	0.2450	

[2] P. Kundur. "*Power system stability and control*," New York: McGraw-Hill, 1994.

[3] X.C. Shangguan, Y. He, C.K. Zhang, et al. "Switching system-based load frequency control for multi-area power system resilient to denial-of-service attacks," *Control Eng. Pract.,* vol. 107, pp. 104678, 2020.

[4] A. Kasis, S. Timotheou, M. Polycarpou, "Optimal secondary frequency regulation with on-off loads in power networks," *IEEE Trans. Control Syst. Technol.,* vol. 30, no. 6, pp. 2490-2505, 2022.

[5] H. Bevrani. *"Robust power system frequency control,"* New York: Springer, 2009.

[6] C. Lin, B. Hu, C. Shao, et al. Delay-dependent optimal load frequency control for sampling systems with demand response," *IEEE Trans. Power Syst.,* vol. 37, no. 6, pp. 4310-4324, 2022.

[7] L. Jiang, W. Yao, Q.H. Wu, et al. "Delay-dependent stability for load frequency control with constant and time-varying delays," *IEEE Trans. Power Syst.,* vol. 27, no. 2, pp. 932-941, 2012.

[8] C.K. Zhang, L. Jiang, Q.H. Wu, et al. "Further results on delay-dependent stability of multi-area load frequency control," *IEEE Trans. Power Syst.,* vol. 28, no. 4, pp. 4465-4474, 2013.

[9] S. Bhowmik, K. Tomsovic, A. Bose, "Communication models for third party load frequency control," *IEEE Trans. Power Syst.,* vol. 19, no. 1, pp. 543-548, 2004.

[10] C. Peng, J. Zhang, "Delay-distribution-dependent load frequency control of power systems with probabilistic interval delays," *IEEE Trans. Power Syst.,* vol. 31, no. 4, pp. 3309-3317, 2016.

[11] W. Yao, L. Jiang, J. Wen, et al. "Wide-area damping controller of FACTS devices for inter-area oscillations considering communication time delays," *IEEE Trans. Power Syst.,* vol. 29, no. 1, pp. 318-329, 2014.

[12] X.C. Shangguan, Y. He, C.K. Zhang, et al. "Control performance standards-oriented event-triggered load frequency control for power systems under limited communication bandwidth," *IEEE Trans. Control Syst. Technol.,* vol. 30, no. 2, pp. 860-868, 2022.

[13] N. Jaleeli, L.S. VanSlyck, "NERC's new control performance standards," *IEEE Trans. Power Syst.,* vol. 14, no. 3, pp. 1092-1099, 1999.

[14] Y. Cao, C. Li, T. He, et al. "A novel Rekasius substitution based exact method for delay margin analysis of multi-area load frequency control systems," *IEEE Trans. Power Syst.,* vol. 36, no. 6, pp. 5222-5234, 2021.

[15] S. Sonmez, S. Ayasun, C.O. Nwankpa, "An exact method for computing delay margin for stability of load frequency control systems with constant communication delays," *IEEE Trans. Power Syst.,* vol. 31, no. 1, pp. 370-377, 2016.

[16] M. Kumar, Y. V. Hote, "Robust PIDD2 controller design for perturbed load frequency control of an interconnected time-delayed power systems," *IEEE Trans. Control Syst. Technol.,* vol. 29, no. 6, pp. 2662-2669, 2021.

[17] C. Peng, J. Li, M. Fei, "Resilient event-triggering H_∞ load frequency control for multi-area power systems with energy-limited DoS attacks," *IEEE Trans. Power Syst.,* vol. 32, no. 5, pp. 4110-4118, 2017.

[18] H. Luo, I.A. Hiskens, Z. Hu, "Stability analysis of load frequency control systems with sampling and transmission delay," *IEEE Trans. Power Syst.,* vol. 35, no. 5, pp. 3603-3615, 2020.

[19] Y. Zhao, W. Yao, C.K. Zhang, et al. "Quantifying resilience of wide-area damping control against cyber attack based on switching system theory," *IEEE Trans. Smart Grid,* vol. 13, no. 3, pp. 2331-2343, 2022.

[20] H. Luo, Z. Hu, "Stability analysis of sampled-data load frequency control systems with multiple delays," *IEEE Trans. Control Syst. Technol.,* vol. 30, no. 1, pp. 434-442, 2022.

[21] Y. He, Q.G. Wang, L.H. Xie, et al. "Further improvement of free-weighting matrices technique for systems with time-varying delay," *IEEE Trans. Autom. Control*, vol. 52, no. 2, pp. 293-299, 2007.

[22] X.L. Zhu, G.H. Yang, "Jensen inequality approach to stability analysis of discrete-time systems with time-varying delay," *American Control Conference*, pp. 1644-1649, 2008.

[23] K.S. Ko, D.K. Sung, "The effect of EV aggregators with time-varying delays on the stability of a load frequency control system," *IEEE Trans. Power Syst.,* vol. 33, no. 1, pp. 669-680, 2018.

[24] A. Seuret, F. Gouaisbaut, "Wirtinger-based integral inequality: Application to time-delay systems," *Automatica*, vol. 49, pp. 2860-2866, 2013.

[25] F. Yang, J. He, D. Wang, "New stability criteria of delayed load frequency control systems via infinite-series-based inequality," *IEEE Trans. Ind. Inf.,* vol. 14, no. 1, pp. 231-240, 2018.

[26] F. Yang, J. He, Q. Pan, "Further improvement on delay-dependent load frequency control of power systems via truncated B-L inequality," *IEEE Trans. Power Syst.,* vol.33, no. 5, pp. 5062-5071, 2018.

[27] S.J Zhou, H.B Zeng, H.Q Xiao, "Load frequency stability analysis of time-delayed multi-area power systems with EV aggregators based on Bessel-Legendre inequality and model reconstruction technique," *IEEE Access.* vol. 8, pp. 99948-99955, 2020.

[28] C.C. Hua, Y.B. Wang, "Delay-dependent stability for load frequency control system via linear operator inequality," *IEEE Trans. Cybern.,* vol. 52, no. 7, pp. 6984-6992, 2022.

[29] M. Zhou, J.F. Yan, "A new solution architecture for online power system analysis," *CSEE J. Power Energy Syst.*, vol. 4, no. 2, pp, 49-55, 2018.

[30] M. Zhou, D.H. Feng, "A new modeling approach for power grid online analysis," *IFAC PapersOnLine*, vol. 53, no,2, pp. 13131-13136, 2020.

[31] L. Jin, Y. He, C.K. Zhang, et al. "Novel structure-exploiting techniques based delay-dependent stability analysis of multi-area LFC with improved numerical tractability," *IEEE Trans. Power Syst.,* vol. 36, no.5, pp. 4194-4211, 2021.

[32] L. Jin, Y. He, C.K. Zhang, et al. "Robust delay-dependent load frequency control of wind power system based on a novel reconstructed model," *IEEE Trans. Cybern.,* vol.52, no. 8, pp. 7825-7836, 2022.

[33] C. Duan, C.K. Zhang, L. Jiang, et al. "Structure-exploiting delay-dependent stability analysis applied to power system load frequency control," *IEEE Trans. Power Syst.,* vol. 32, no. 6, pp. 4528-4540, 2017.

[34] L. Jin, C.K. Zhang, Y. He, et al. "Delay-dependent stability analysis of multi-area load frequency control with enhanced accuracy and computation efficiency," *IEEE Trans. Power Syst.,* vol. 34, no. 5, pp. 3687-3696, 2019.

[35] T. Athay, R. Podmore, S. Virmani, "A practical method for the direct analysis of transient stability," *IEEE Trans. Power App. Syst.,* vol. PAS-98, no. 2, pp. 573-584, 1979.

[36] L. Jin, Y. He, L. Jiang, "A novel integral inequality and its application to stability analysis of linear system with multiple time delays," *Appl. Math. Lett.,* 124: 107648, 2021.